Supplementary Information

Different brain regions support deliberation during food choice in disordered and healthy eating

Authors: Alexandra F. Muratore[1], Eileen A. Hartnett[2], Karin Foerde[1,3], Blair W. Uniacke[1], B. Timothy Walsh[1], Joanna Steinglass[1], Daphna Shohamy[2,4], Akram Bakkour[2,5]

Affiliations:

[1]New York State Psychiatric Institute and Department of Psychiatry, Columbia University Irving Medical Center, New York, NY 10032, USA.

[2]Department of Psychology and Mortimer B. Zuckerman Mind Brain Behavior Institute, Columbia University, New York, NY 10027, USA.

[3]Department of Psychology, University of Amsterdam, Amsterdam, the Netherlands.

[4]The Kavli Institute for Brain Science, Columbia University, New York, NY 10027, USA.

[5]Department of Psychology, Institute for Mind and Biology, and Neuroscience Institute, University of Chicago, Chicago, IL 60637, USA.

Correspondence: afm2166@cumc.columbia.edu (AFM) and bakkour@uchicago.edu (AB)

I. fMRI preprocessing

Anatomical data preprocessing

One T1-weighted (T1w) image was corrected for intensity non-uniformity (INU) with `N4BiasFieldCorrection`[1], distributed with ANTs 2.3.3 (Avants et al. 2008, RRID:SCR_004757). The T1w-reference was then skull-stripped with a *Nipype* implementation of the `antsBrainExtraction.sh` workflow (from ANTs), using OASIS30ANTs as target template. Brain tissue segmentation of cerebrospinal fluid (CSF), white-matter (WM) and gray-matter (GM) was performed on the brain-extracted T1w using `fast` (FSL 5.0.9, RRID:SCR_002823[2]). A T1w reference map was computed after registration of 2 T1w images (after INU-correction) using `mri_robust_template` (FreeSurfer 6.0.1[3]). Brain surfaces were reconstructed using `recon-all` (FreeSurfer 6.0.1, RRID:SCR_001847[4]), and the brain mask estimated previously was refined with a custom variation of the method to reconcile ANTs-derived and FreeSurfer-derived segmentations of the cortical gray-matter of Mindboggle (RRID:SCR_002438[5]). Volume-based spatial normalization to one standard space (MNI152NLin2009cAsym) was performed through nonlinear registration with `antsRegistration` (ANTs 2.3.3), using brain-extracted versions of both T1w reference and the T1w template. The following template was selected for spatial normalization: *ICBM 152 Nonlinear Asymmetrical template version 2009c*[6] (RRID:SCR_008796; TemplateFlow ID: MNI152NLin2009cAsym).

Functional data preprocessing

For each of the 6 BOLD runs per participant (across all tasks), the following preprocessing was performed. First, a reference volume and its skull-stripped version were generated using a custom methodology of *fMRIPrep*. A B0-nonuniformity map (or *fieldmap*) was estimated based on two (or more) echo-planar imaging (EPI) references with opposing phase-encoding directions, with `3dQwarp`[7] (AFNI 20160207). Based on the estimated susceptibility distortion, a corrected EPI (echo-planar imaging) reference was calculated for a more accurate co-registration with the anatomical reference. The BOLD reference was then co-registered to the T1w reference using `bbregister` (FreeSurfer) which implements boundary-based registration[8]. Co-registration was configured with six degrees of freedom. Head-motion parameters with respect to the BOLD reference (transformation matrices, and six corresponding rotation and translation parameters) are estimated before any spatiotemporal filtering using `mcflirt` (FSL 5.0.9[9]). BOLD runs were slice-time corrected to 0.708s (0.5 of slice acquisition range 0s-1.42s) using `3dTshift` from AFNI 20160207[7], RRID:SCR_005927. The BOLD time-series (including slice-timing correction when applied) were resampled onto their original, native space by applying a single, composite transform to correct for head-motion and susceptibility distortions. These resampled BOLD time-series will be referred to as *preprocessed BOLD in original space*, or just *preprocessed BOLD*. The BOLD time-series were resampled into standard space, generating a *preprocessed BOLD run in MNI152NLin2009cAsym space*. First, a reference volume and its skull-stripped version were generated using a custom methodology of *fMRIPrep*. Several confounding time-series were calculated based on the *preprocessed BOLD*: framewise displacement (FD), DVARS and three region-wise global signals. FD was computed using two formulations following Power (absolute sum of relative motions[10]) and Jenkinson (relative root mean square displacement between affines[9]). FD and DVARS are calculated for each functional run, both using their implementations in *Nipype* (following the definitions by Power et al.[10]). The three global signals are extracted within the CSF, the WM, and the whole-brain

masks. Additionally, a set of physiological regressors were extracted to allow for component-based noise correction (*CompCor*[11]). Principal components are estimated after high-pass filtering the *preprocessed BOLD* time-series (using a discrete cosine filter with 128s cut-off) for the two *CompCor* variants: temporal (tCompCor) and anatomical (aCompCor). tCompCor components are then calculated from the top 2% variable voxels within the brain mask. For aCompCor, three probabilistic masks (CSF, WM and combined CSF+WM) are generated in anatomical space. The implementation differs from that of Behzadi et al.[11] in that instead of eroding the masks by pixels on BOLD space, the aCompCor masks are subtracted a mask of pixels that likely contain a volume fraction of GM. This mask is obtained by dilating a GM mask extracted from the FreeSurfer's *aseg* segmentation, and it ensures components are not extracted from voxels containing a minimal fraction of GM. Finally, these masks are resampled into BOLD space and binarized by thresholding at 0.99 (as in the original implementation). Components are also calculated separately within the WM and CSF masks. For each CompCor decomposition, the *k* components with the largest singular values are retained, such that the retained components' time series are sufficient to explain 50 percent of variance across the nuisance mask (CSF, WM, combined, or temporal). The remaining components are dropped from consideration. The head-motion estimates calculated in the correction step were also placed within the corresponding confounds file. The confound time series derived from head motion estimates and global signals were expanded with the inclusion of temporal derivatives and quadratic terms for each[12]. Frames that exceeded a threshold of 0.5 mm FD or 1.5 standardized DVARS were annotated as motion outliers. All resamplings can be performed with *a single interpolation step* by composing all the pertinent transformations (i.e. head-motion transform matrices, susceptibility distortion correction when available, and co-registrations to anatomical and output spaces). Gridded (volumetric) resamplings were performed using `antsApplyTransforms` (ANTs), configured with Lanczos interpolation to minimize the smoothing effects of other kernels[13]. Non-gridded (surface) resamplings were performed using `mri_vol2surf` (FreeSurfer). First, a reference volume and its skull-stripped version were generated using a custom methodology of *fMRIPrep*. A B0 nonuniformity map (or *fieldmap*) was estimated based on a phase-difference map calculated with a dual-echo GRE (gradient-recall echo) sequence, processed with a custom workflow of *SDCFlows* inspired by the `epidewarp.fsl` script and further improvements in HCP Pipelines[14]. The *fieldmap* was then co-registered to the target EPI (echo-planar imaging) reference run and converted to a displacements field map (amenable to registration tools such as ANTs) with FSL's `fugue` and other *SDCflows* tools. Based on the estimated susceptibility distortion, a corrected EPI (echo-planar imaging) reference was calculated for a more accurate co-registration with the anatomical reference. We did not acquire fieldmaps on all participants. For those participants missing a fieldmap, no fieldmap correction was performed within *fMRIPrep*. All other pre-processing steps for these participants were the same as those indicated above.

Many internal operations of *fMRIPrep* use *Nilearn* 0.6.2[15], RRID:SCR_001362, mostly within the functional processing workflow. For more details of the pipeline, see the section corresponding to workflows in *fMRIPrep*'s documentation.

II. Participant Characteristics

Table S1: Participant clinical characteristics.

	HC (n = 29)	AN (n = 28) / Atypical AN (n = 2)			
	Mean ± SD	Mean ± SD	t	df	p
Age (years)	25.13 ± 4.85 (18-37)	24.50 ± 6.52 (16-41)	0.43	53.54	0.67
BMI (kg/m^2)	21.75 ± 1.62 (19.1-24.5)	17.48 ± 1.73 (14.5-21)	9.70	55.74	<.001
Subtype					
Restricting / Binge-purge	-	n = 16 / 14	-	-	-
Duration of Illness (years)	-	7.37 ± 7.18 (0.25-23)	-	-	-
EDE-Q, Global Score	0.23 ± 0.31(0-1.1)	4.42 ± 1.07 (1.39-5.9)	-20.44	34.74	<.001
TFEQ-R	4.37 ± 3.43 (0-16)	18.62 ± 2.82 (12-21)	-16.90	50.46	<.001
STAI-T	29.92 ± 7.54 (20-51)	62.55 ± 9.66 (39-80)	-13.93	51.53	<.001
BDI	1.35 ± 2.11 (0-7)	31.53 ± 9.82 (8-47)	-16.20	30.58	<.001
WASI-II FSIQ	114.48 $\pm$ 9.12 (101-140)	107.97 $\pm$ 2.48 (79-135)	2.17	50.91	.04
Race/Ethnicity	n (%)	n (%)			
African American	3 (10%)	0 (0%)			
Asian	11 (38%)	2 (.07%)			
Caucasian	10 (35%)	24 (80%)			
Hispanic	4 (14%)	3 (.1%)			
Biracial	1 (3%)	1 (.03%)			

BMI = Body Mass Index at time of study, EDE-Q = Eating Disorder Examination Questionnaire (value missing for 4 HC), TFEQ-R = Three Factor Eating Questionnaire, Restraint Scale (value missing for 2 HC and 1 AN), STAI-T = Spielberger Anxiety Index, Trait version (value missing for 4 HC and 1 AN); BDI = Beck Depression Index (value missing for 1 AN); WASI-II FSIQ = Wechsler Abbreviated Scale of Intelligence, 2nd edition, Full Scale IQ score. Values were compared between groups using Welch's t-test.

III. Behavioral Analyses

Figure S1. Distribution of baseline preference ratings across both groups.

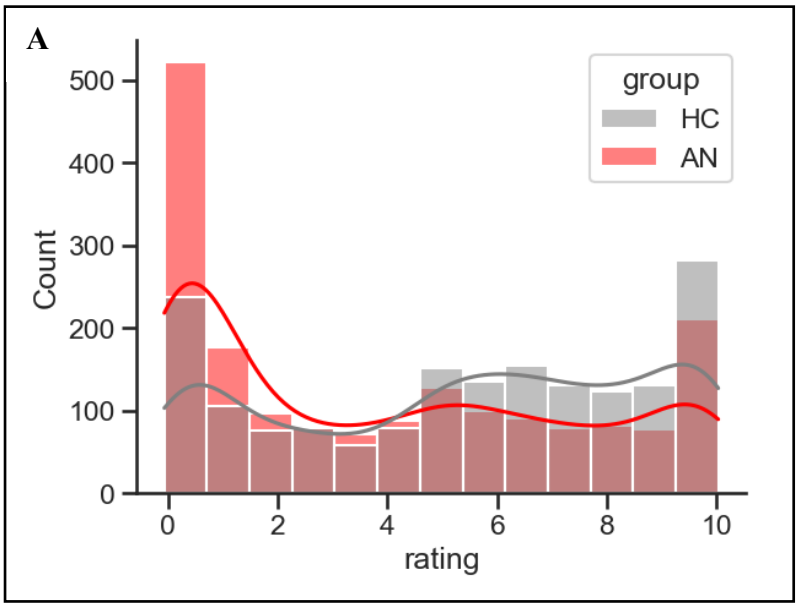

Figure S2. Distribution of delta value across groups.

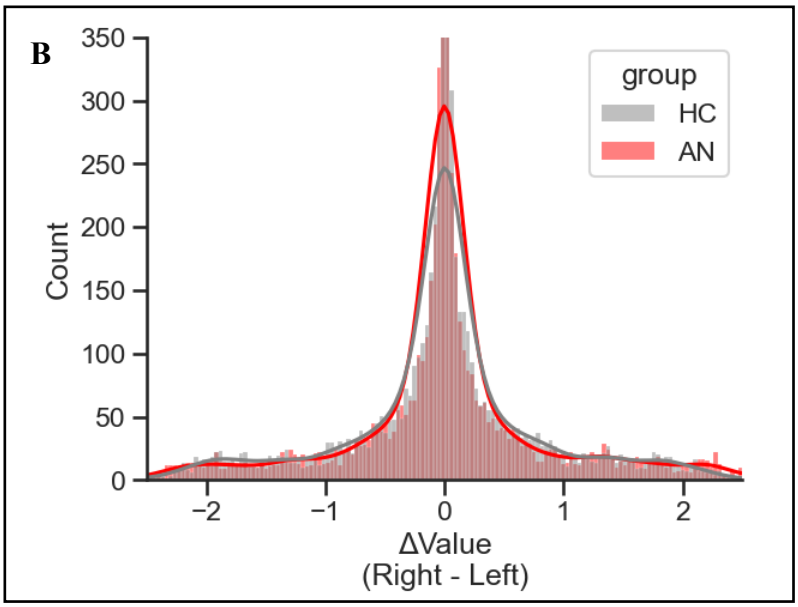

Table S2. Regression results for choice and reaction time during food choice task

	Chose Right			RT		
	Odds Ratio	*CI*	*p*	*β*	*CI*	*p*
Intercept	0.94	0.86 – 1.02	0.12	1.38	1.33 – 1.43	**<0.001**
ΔValue	5.83	4.33 – 7.85	**<0.001**	-0.11	-0.13 – -0.08	**<0.001**
Group [HC]	0.91	0.81 – 1.03	0.128	-0.05	-0.12 – 0.03	0.215
Avg Value	0.97	0.91 – 1.03	0.346	-0.11	-0.12 – -0.09	**<0.001**
ΔValue × Group	0.88	0.58 – 1.32	0.524	0.04	0.00 – 0.07	**0.026**
ΔValue × Avg Value	1.17	0.93 – 1.46	0.178	0	-0.02 – 0.02	0.971
Group × Avg Value	1.03	0.95 – 1.12	0.483	0.04	0.02 – 0.07	**0.002**
ΔValue × Group × Avg Value	0.99	0.74 – 1.33	0.958	0	-0.03 – 0.03	0.833
N	59			59		
Observations	11847			11847		
Marginal R^2	0.357			0.081		
Conditional R^2	0.426			0.214		

Note: for RT regression, Δ*Value* is entered as absolute value of signed Δ*Value*. Avg Value is included to account for differences in overall value, but its effect on behavior is not discussed.

Table S3. Regression results for choice and reaction time during perceptual choice task

	Chose Blue			RT		
	Odds Ratio	*CI*	*p*	*β*	*CI*	*p*
Intercept	1.66	1.26 – 2.18	**<0.001**	1.12	1.04 – 1.20	**<0.001**
Color Coherence	24.77	12.65 – 48.48	**<0.001**	-0.17	-0.21 – -0.13	**<0.001**
Group [HC]	0.83	0.56 – 1.22	0.347	0.02	-0.09 – 0.13	0.744
Color Coherence × Group	2.36	0.90 – 6.20	0.08	-0.02	-0.07 – 0.04	0.586
N	59			59		
Observations	11956			11956		
Marginal R^2	0.622			0.086		
Conditional R^2	0.801			0.308		

Note: for RT regression, Color Coherence is entered as absolute value of signed Color Coherence

IV. Imaging Analyses

A. Effect of mean value of food items

A1. Whole Brain Analysis

Table S4. Activation table for effect of the mean value of food items in HC and patients with AN within the whole-brain. The uncorrected map is available for HC here: https://neurovault.org/collections/RGDXSBMN/images/803571/ and for patients here: https://neurovault.org/collections/RGDXSBMN/images/803572/.

Group	Region	# Voxels	x	y	z	peak Z	p
AN	vmPFC	42	-10.5	67.5	7.5	4.11	0.021

A2. Small-Volume Correction

Table S5. Activation table for effect of the mean value of the food items in HC and patients with AN within the ventromedial prefrontal cortex.

Group	SVC Region	# Voxels	x	y	z	peak Z	p
HC	vmPFC	43	-4.5	39.5	-4.5	3.69	0.015
AN	vmPFC	52	-6.5	45.5	-8.5	3.49	0.008

B. Effect of RT during value-based versus perceptual-based decisions

B1. Whole Brain Analysis

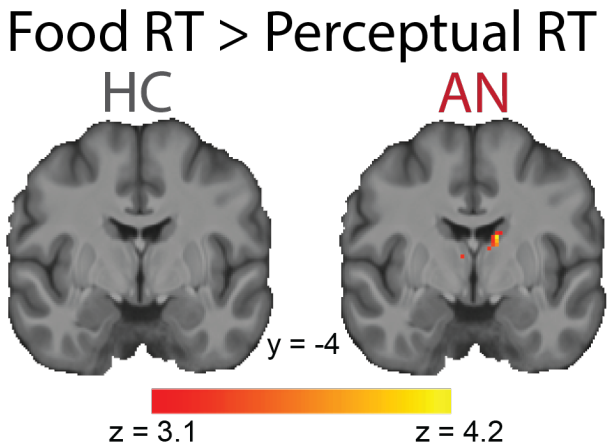

Figure S3. Whole-Brain activation map for effect of RT during value-based vs perceptual decisions (food > perceptual) in HC and patients with AN. The uncorrected map for HC is available here: https://neurovault.org/collections/RGDXSBMN/images/803497/ and the uncorrected map for patients is available here: https://neurovault.org/collections/RGDXSBMN/images/803498/.

Table S6. Activation table for effect of RT during value-based vs. perceptual decisions (food > dots) in HC and patients with AN.

Group	Region	# Voxels	x	y	z	peak Z	p
HC	R Lateral Occipital Cortex	99	31.5	-96.5	-0.5	3.84	<.0001
	R Superior Frontal Gyrus/Middle Frontal Gyrus	55	23.5	39.5	45.5	4.16	0.003
AN	L Lateral Occipital Cortex	233	-28.5	-100	-6.5	4.83	<.0001
	R Lateral Occipital Cortex	209	31.5	-94.5	-10.5	5.94	<.0001
	L Caudate/Thalamus	197	-12.5	-8.5	15.5	4.55	<.0001
	R Cerebellum	103	15.5	-84.5	-22.5	5.03	<.0001
	L Superior Frontal Gyrus	96	-8.5	27.5	39.5	5.02	<.0001
	L Orbital Frontal Cortex	61	-34.5	35.5	-18.5	4.61	0.002
	R Cerebellum	57	33.5	-66.5	-28.5	4.14	0.003
	L Cuneus	38	-12.5	-84.5	3.5	4.52	0.030
	L Lingual Gyrus	37	-12.5	-76.5	-10.5	3.86	0.034
	R Cuneus	37	15.5	-84.5	5.5	4.12	0.034
	R Lingual Gyrus	35	29.5	-54.5	-4.5	4.19	0.045

B2. Small-Volume Correction

Table S7. Activation table for effect of RT during value-based vs. perceptual decisions (food > dots) in HC and patients with AN using small-volume correction within the striatum and hippocampus, pre-registered model.

Group	SVC Region	# Voxels	X	y	Z	peak Z	p
AN	Striatum	11	-12.5	-4.5	17.5	4.13	0.036
		10	29.5	-6.5	9.5	4.19	0.044
	Hippocampus	12	-18.5	-10.5	-24.5	4.31	0.016

V. PPI Analysis

A. Whole Brain Analysis

Table S8. Activation table for whole-brain PPI analysis using dorsal striatum as a seed. The uncorrected map is available for HC here: https://neurovault.org/collections/RGDXSBMN/images/803599/ and for patients here: https://neurovault.org/collections/RGDXSBMN/images/803600/.

Group	Region	# Voxels	x	y	z	peak Z	p
AN	Bilateral Dorsal Medial Prefrontal Cortex	142	-6.5	49.5	35.5	3.89	<.0001

B. Small-Volume Correction

Table S9. Activation table for small-volume corrected PPI analysis using dorsal striatum as a seed and dlPFC as ROI.

Group	Region	# Voxels	x	y	z	peak Z	p
AN	Bilateral Dorsal Medial Prefrontal Cortex	48	-6.5	63.5	3.5	4.65	.002

VI. Pre-registered hypotheses

Table S10. Pre-registered hypotheses and corresponding results.

Pre-registered Hypothesis	Result
Behavior on the food choice task will differ between patients with AN and HC.	The results (**Figure 2B, Table S2**) do not support this hypothesis.
Behavior on the perceptual task will be the same for patients with AN and HC.	The results (**Figure 3, Table S3**) support this hypothesis.
Eyetracking will reveal differences in gaze patterns in patients with AN and HC.	This hypothesis was not tested due to eyetracking data quality issues.
RT will correlate more positively with BOLD activity in the striatum during decisions about food compared to perceptual decisions in patients with AN.	The ROI analysis results (**Figure 4C**) and whole-brain fMRI analysis (**Figure S3**) support this hypothesis. The same effect was also found in the hippocampus (**Figures 4B, S3**). The effect in the hippocampus did not survive whole brain correction (**Table S6**).
RT will correlate more positively with BOLD activity in the hippocampus during food-based compared to perceptual decisions in HC.	The ROI analysis results (**Figure 4B**) support this hypothesis, but the effect did not survive whole-brain correction for multiple comparisons (**Table S6**).
Functional connectivity between striatum and dlPFC will increase with RT during food choice compared to perceptual choice in patients with AN.	The results support this hypothesis (**Figure 5** & **Tables S8, S9**).
Functional connectivity between striatum and vmPFC will increase with RT during food choice compared to perceptual choice in HC.	The results do not support this hypothesis (**Table S8)**.

References

1. Tustison NJ, Avants BB, Cook PA, Zheng Y, Egan A, Yushkevich PA, et al. N4ITK: Improved N3 Bias Correction. IEEE Trans Méd Imaging. 2010;29:1310–1320.

2. Zhang Y, Brady M, Smith S. Segmentation of brain MR images through a hidden Markov random field model and the expectation-maximization algorithm. IEEE Trans Méd Imaging. 2001;20:45–57.

3. Reuter M, Rosas HD, Fischl B. Highly accurate inverse consistent registration: a robust approach. NeuroImage. 2010;53:1181–1196.

4. Dale AM, Fischl B, Sereno MI. Cortical Surface-Based Analysis: I. Segmentation and Surface Reconstruction. NeuroImage. 1999;9:179–194.

5. Klein A, Ghosh SS, Bao FS, Giard J, Häme Y, Stavsky E, et al. Mindboggling morphometry of human brains. PLoS Comput Biol. 2017;13:e1005350.

6. Fonov VS, Evans AC, McKinstry RC, Almli CR, Collins DL. Unbiased nonlinear average age-appropriate brain templates from birth to adulthood. NeuroImage. 2009;47:S102.

7. Cox RW, Hyde JS. Software tools for analysis and visualization of fMRI data. NMR Biomed. 1997;10:171–178.

8. Greve DN, Fischl B. Accurate and robust brain image alignment using boundary-based registration. NeuroImage. 2009;48:63–72.

9. Jenkinson M, Bannister P, Brady M, Smith S. Improved Optimization for the Robust and Accurate Linear Registration and Motion Correction of Brain Images. NeuroImage. 2002;17:825–841.

10. Power JD, Mitra A, Laumann TO, Snyder AZ, Schlaggar BL, Petersen SE. Methods to detect, characterize, and remove motion artifact in resting state fMRI. NeuroImage. 2014;84:320–341.

11. Behzadi Y, Restom K, Liau J, Liu TT. A component based noise correction method (CompCor) for BOLD and perfusion based fMRI. NeuroImage. 2007;37:90–101.

12. Satterthwaite TD, Elliott MA, Gerraty RT, Ruparel K, Loughead J, Calkins ME, et al. An improved framework for confound regression and filtering for control of motion artifact in the preprocessing of resting-state functional connectivity data. NeuroImage. 2013;64:240–256.

13. Lanczos C. Evaluation of Noisy Data. J Soc Ind Appl Math Ser B Numer Anal. 1964;1:76–85.

14. Glasser MF, Sotiropoulos SN, Wilson JA, Coalson TS, Fischl B, Andersson JL, et al. The minimal preprocessing pipelines for the Human Connectome Project. NeuroImage. 2013;80:105–124.

15. Abraham A, Pedregosa F, Eickenberg M, Gervais P, Mueller A, Kossaifi J, et al. Machine learning for neuroimaging with scikit-learn. Front Neuroinformatics. 2014;8:14.